Improving The Performance Of Dc Motor Drive Application For Dc-Dc Converter By Using Resistance Compression Network

B. Umamaheswara Rao[1], P.Siva Krishna [2] M.Tech

Brahmaiah college of Engineering

Electrical and Electronics Engineering

North Rajupalem,kovur-524137

Email: maheswararao048@gmail.com

Abstract— **In this paper improve the performance of DC motor by the resistance compression network. The output DC supply is dependence upon number of transformer winding ratio. If the DC input side voltage is two times of the output side voltage. The RCN maintains desired current waveforms over a wide range of voltage operating conditions. HIGH-voltage-pick up dc/dc converters are found in a mixed bag of utilizations [1]–[4]. For instance, to associate photovoltaic boards to the lattice, interface hardware is required. A few architectures for this reason consolidate dc/dc converters to support voltage of individual photovoltaic boards to a high dc-join voltage, with take after on gadgets for changing over dc to air conditioning (e.g., see, [5] and [6]). The progression up dc/dc converter is a discriminating piece of this framework, and must work effectively for an extensive voltage venture up and for a wide voltage range (e.g., at the converter information and/or yield contingent on the framework). Moreover, to be minimal, it must work at high exchanging frequencies. In ordinary hard-exchanged force converters, the cover of current and voltage is extensive amid exchanging, bringing about huge force misfortune, particularly at high frequencies. We implementing torque and speed characteristics are performed by the Resistance Compression Network (RCN). The validated results are verified by the MATLAB/SIMULINK Software**

*Index Terms—***DC/DC converter, high-efficiency power con-verter, ON–OFF control, resistance compression network (RCN), resonant converter,dc motor chopper drive.**

I. INTRODUCTION

HIGH-voltage-gain dc/dc converters are found in a varietyof applic ations [1]–[4]. For example, to connect photo-

voltaic panels to the grid, interface circuitry is needed. Some architectures for this purpose incorporate dc/dc converters to boost voltage of individual photovoltaic panels to a high dc-link voltage, with follow-on electronics for converting dc to ac (e.g., see, [5] and [6]). The step-up dc/dc converter is a critical part of this system, and must operate efficiently for a large voltage step up and for a wide voltage range (e.g., at the converter input and/or output depending upon the system). Furthermore, to be compact, it must operate at high switching frequencies.

In conventional hard-switched power converters, the over-lap of current and voltage is large during switching, resulting in significant power loss, especially at high frequencies. Soft-switched resonant converter topologies providing zero-voltage switching (ZVS) or zero-current switching (ZCS) can greatly reduce loss at the switching transitions, enabling high efficiency at high frequencies (e.g., see, [7] and [8]). Unfortunately, while many soft-switched resonant designs achieve excellent perfor-mance for nominal operating conditions, performance can de-grade quickly with variation in input and output voltages and

Limitations on the efficient operating range of resonant con-

verters are tied to both converter structure and control. Numer-ous control techniques are possible for compensating variations in input voltage, output voltage, and power level. These in-clude frequency control [7], [8], phase-shift PWM control [11], asymmetric duty cycle PWM control [12], and ON–OFF or burst mode control [13]. Each of these control techniques in conjunction with conventional resonant tank structures imposes significant design limits. For example, the conventional half-bridge series resonant converter (SRC) [8] requires wide-band frequency variation to control the power when output load or input voltage varies such that the magnetics cannot be opti-mally designed. Furthermore, to maintain ZVS, the frequency must increase to reduce power, hurting the efficiency at light load. For a full-bridge version of the SRC, phase-shift control can be used to control the power and reject conversion ratio variations (e.g., see, [11]). However, this results in asymmet-rical current levels in the switches at the switching instants, with the switches in the leading leg turning OFF at high cur-rents. The effective impedance of the rectifier in a resonant con-verter also often causes challenges, as it varies with operating conditions.

This paper introduces a new high efficiency resonant dc/dc converter topology, the resistance compression network (RCN) converter, which seeks to overcome the aforementioned chal-lenges. This converter operates with simultaneous ZVS and near-ZCS across a wide range of input voltage, output voltage, and power levels, resulting in low switching losses. This study represents an expansion on an earlier conference paper [14], and includes additional experimental results and estimates of loss breakdown.

The remainder of this paper is organized as follows: Section II describes the topology and control of the proposed RCN dc/dc converter. The converter is analyzed and methodology for its design is presented in Section III. Section IV describes the de-sign and implementation of a RCN dc/dc converter.

The simulation results of dc motor chopper drive are present and discussed in Section V. Finally, Section VI summarizes the conclusion of the paper. The equations used to esti-mate the losses in the various components are given in an Appendi
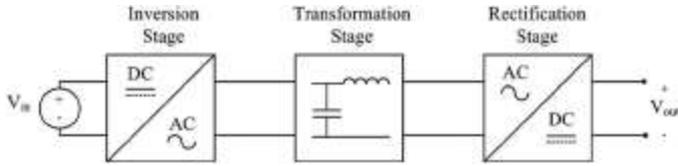
Fig. 1. Architecture of the proposed dc/dc converter.
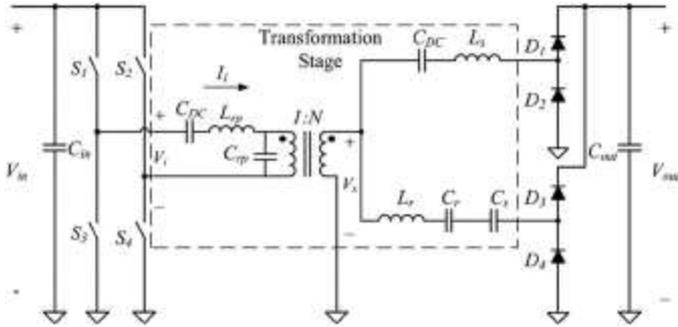
Fig. 2. Topology of the proposed RCN dc/dc converter.

II. RCN CONVERTER TOPOLOGY AND CONTROL

The dc/dc converter proposed here consists of an inversion stage, a transformation stage, and a rectification stage, as shown in Fig. 1. The inversion and rectification stages use standard designs. However, the transformation stage and the control of the converter are new. The topology of the proposed RCN converter is shown in Fig. 2. The converter as shown is designed to step-up voltage. The transformation stage consists of a matching network, a transformer, and an RCN. The matching network composed of L_{rp} and C_{rp} acts as a filter and provides a voltage gain [17], hence reducing the transformer turns ratio requirement. One issue with high-turns-ratio step-up transformers that exists in many topologies is that the parasitic leakage inductance of the transformer can undesirably ring with its secondary side winding capacitance at the switching transitions. This creates large ringing in the current and voltage waveforms, and high-frequency losses. The matching network also eliminates this ringing by absorbing the transformer parasitics. The 1:N transformer provides additional voltage gain and isolation. The RCN (composed of L_s and C_s) is a special single input, multioutput matching network that provides desirable impedance control characteristics [15], [16], [23]. The RCN technique was originally proposed and applied for radio-frequency (RF) applications, such as very-high-frequency dc/dc converter systems [15] and RF power amplifiers [16]; here, we exploit if for high efficiency power conversion. The function of the RCN is to automatically regulate the converter operating power and waveforms in a desirable manner as the input and output voltages vary. As applied here, the RCN also includes a series resonant tank (composed of L_r and C_r) [8]. Its purpose is to provide additional filtering. The inverter stage is simply a full-bridge inverter (composed of switches $S_1 - S_4$). A full bridge is used instead of a half bridge to reduce the voltage gain requirement from the matching network and the transformer. The rectification stage is composed of two half-bridge rectifiers. The capacitors C_{in} and
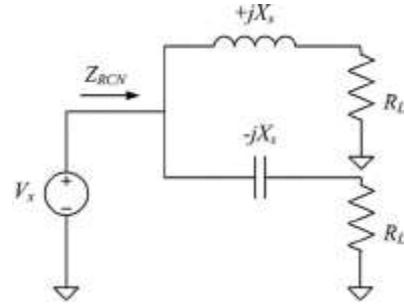
Fig. 3. Fundamental frequency model of the RCN and the rectifiers.

C_{out} are for input and output filtering, respectively, and the two capacitors marked as C_{DC} are for dc blocking purposes.

The output power in the proposed converter is regulated using ON–OFF control, also known as burst-mode control or bang–bang control. The power is controlled by gating the converter ON and OFF at a modulation frequency that is much lower than the switching frequency [13], [15], [21]. The advantage of using ON–OFF control is that the magnetics are designed for only a single frequency (a high frequency), while the power is regulated by turning the converter ON and OFF at a lower frequency. Moreover, the power is transferred only in the fraction of the time the converter is ON, which results in high efficiency even at light loads. The output power is controlled by the duty ratio of the ON–OFF modulation. The ON–OFF control can be implemented through hysteretic control (e.g., see, [18]–[20]), through fixed-period ON–OFF PWM (e.g., see, [21]), or other methods. Additional care may be necessary in implementations that allow very short ON or OFF durations to maintain high efficiency and desired operation during ON–OFF transient conditions.

The ON–OFF modulation has its own corresponding loss. The higher the modulation frequency the greater the loss. The output capacitance is sized according to the ON–OFF modulation frequency; with a lower modulation frequency, a larger capacitor has to be used. The duty ratio of the modulation also influences the loss. Very small or very large duty ratio results in greater loss as the converter operates in steady state for a shorter time. So, in order to minimize the total loss both the modulation frequency and the duty ratio have to be considered.

III. ANALYSIS AND DESIGN METHODOLOGY

Using fundamental frequency analysis, at the switching frequency the half-bridge rectifiers can be modeled as resistors [8], [16], as illustrated in Fig. 3. The effective resistance of these rectifiers is given by

$$R_L = \frac{4V_{out}^2}{\pi^2 P_{out}} \tag{1}$$

where V_{out} is the converter output voltage and P_{out} is the switching-cycle-average output power. As shown in Fig. 2, one of the branches of the RCN comprises a blocking capacitor C_{DC} and an RCN inductor L_s. The other branch comprises a series LC tank tuned to be net capacitive at the switching frequency (net equivalent capacitance C_s). This branch may be modeled as a series resonant tank (with components L_r and C_r) tuned
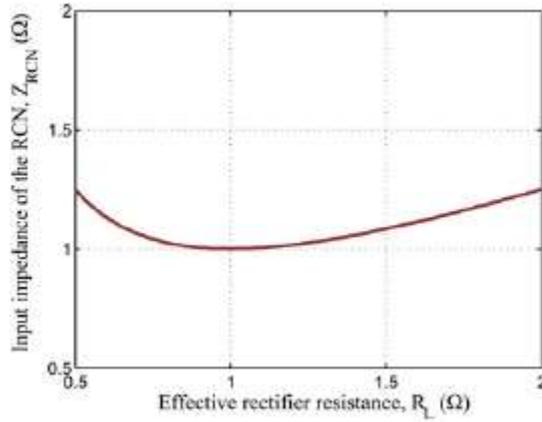
Fig. 4. Variation in the resistive input impedance of the RCN (Z_{RCN}) as a function of the effective rectifier resistance (R_L). Z_{RCN} is plotted assuming the reactance X_s has a value of 1 Ω.

Fig. 5. Matching network with equivalent impedance.

Fig. 6. Implementation of the proposed RCN dc/dc converter.

to the switching frequency for filtering, in series with an additional RCN capacitance C_s. Since the series LC tank appears as a short circuit at the switching frequency, it is treated as such in Fig. 3 and in the following analysis. Similarly, the dc blocking capacitor C_{DC} of Fig. 2 is an effective short at the high switching frequency. Hence, at the switching frequency the input impedance of the RCN looks purely resistive and is given by

$$Z_{RCN} = \frac{X_s^2 + R_L^2}{2R_L} \quad (2)$$

where X_s is the magnitude of impedance of the RCN elements (L_s and C_s) at the switching frequency. The use of the RCN reduces the change in impedance seen by the inverter as the effective rectifier resistance (R_L) changes due to variations in output voltage and output power [15], [16]. This compression effect can be seen in Fig. 4, which shows that the RCN input impedance (Z_{RCN}) varies only by 25%, while the effective rectifier resistance varies by 400%. This helps achieve ZVS and near-ZCS of the inverter switches across a wide range of output and input voltages. The RCN also serves to limit the instantaneous output power across the full operating range by providing a specified loading characteristic to the inverter. The value of X_s is selected in such a way so as to limit the output power to the maximum value required across the range of output voltages at the minimum input voltage. Since the power delivery capability of the converter increases with input voltage, this ensures that the converter can deliver the maximum required power across its entire input voltage range. It is also noted that the power characteristic across output voltage is quite flat at the minimum input voltage, owing to the effect of the RCN. The expression for output power (P_{out}) can be found by neglecting losses and equating input power ($P_{in} = (\frac{4}{\pi} V_{in})^2 / 2Z_I$, where Z_I is the input impedance of the matching network as shown in Fig. 5) to output power ($P_{out} = 4V_{out}^2/\pi^2 R_L$). The output power of the converter is given by

$$P_{out} = \frac{4V_{out}}{X_s \pi^2} \sqrt{4V_{in}^2 N^2 G^2 - V_{out}^2}.$$
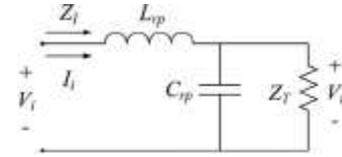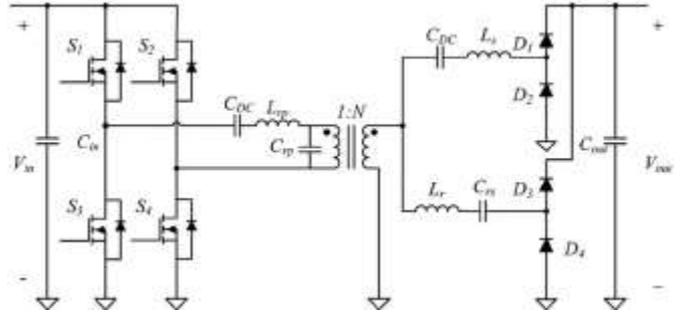
This expression for output power is in terms of input voltage (V_{in}), output voltage (V_{out}), the transformer turns ratio (N) and the matching network gain voltage (G).

The gain of the matching network can be calculated using the equivalent circuit of Fig. 5 and is given by

$$G \equiv \frac{V_t}{V_i} = \frac{1}{\left(\frac{\omega L_{rp}}{Z_T}\right)^2 + (1 - \omega^2 L_{rp} C_{rp})^2} \quad (4)$$

where ω is the angular switching frequency. Here, Z_T ($= Z_{RCN}/N^2$) is the effective load seen by the matching network. As Z_T varies with changes in power, the gain varies. However, due to the RCN, this gain is fairly constant across variation in input and output voltages. The input impedance of the matching network as seen by the inverter is given by

$$Z_I = \frac{j(X_{Lrp}Z_T^2 + X_{Crp}^2 X_{Lrp} - X_{Crp}Z_T^2) + X_{Crp}^2 Z_T}{Z_T^2 + X_{Crp}^2} \quad (5)$$

where X_{Lrp} and X_{Crp} are the magnitude of the impedance of L_{rp} and C_{rp}, respectively. For Z_I to be resistive, X_{Lrp}, X_{Crp}, and Z_T must satisfy

$$X_{Lrp} = \frac{X_{Crp} Z_T^2}{X_{Crp}^2 + Z_T^2}. \quad (6)$$

Picking X_{Lrp} to be slightly larger than the value given by (6) so that Z_I is slightly inductive, ensures that the inverter switches achieve ZVS and near-ZCS. The application of the equations presented previously is illustrated in the design of the dc/dc converter in the next section..

IV. SIMULINK CONVETER DESIGN

The RCN network and dc motor chopper drive has been designed and built. The designed dc/dc converter is meant for large-step-up applications such as the two-stage photovoltaic-to-grid conversion system shown in Fig. 7. The RCN dc/dc converter can be used to convert the low (widely varying) output
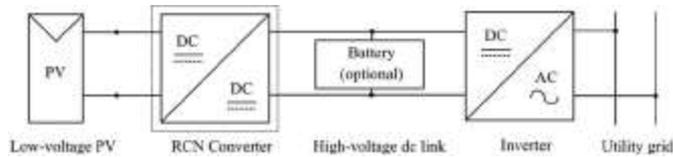
Fig. 7.   Block diagram of a grid-connected PV system.

TABLE I
SPECIFICATIONS FOR THE DC/DC CONVERTER

Parameter	Value
Input Voltage (V_{in}) Range	25 V - 40 V
Output Voltage (V_{out}) Range	250 V - 400 V
Output Power (P_{out}) Range	20 W - 200 W
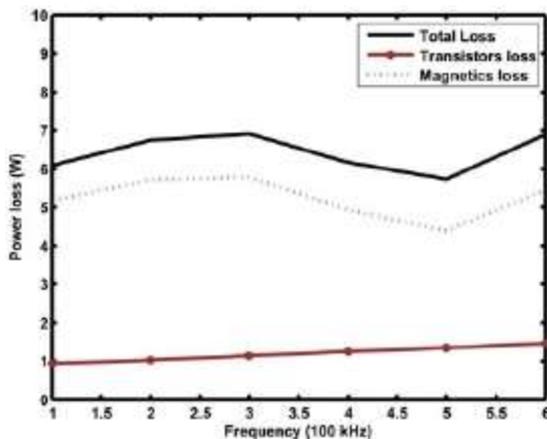
Fig. 8.   Power loss in the converter (in magnetics and mosfet) with varying frequency when the converter is soft-switched.

Fig:-simulink type RCN type dc/dc converter

Fig:-simulink type chopper DC drive

voltage of a photovoltaic panel into a high dc-link voltage The converter is required to operate over an input. voltage range of 25–40 V, an output voltage range of 250–400 V and over a wide output power range of 20–200 W.

The switching frequency of the converter was selected as 500 kHz. This frequency minimized the total losses in the magnetics (assuming 3F3 magnetic material and RM cores) and the mosfets as shown in Fig. 8. Given that the architecture provides relatively low mosfet switching losses, selection of a different magnetic material could enable significantly higher frequencies to be utilized. The ON/OFF modulation frequency for output power control was chosen as 500 Hz. The reason for selecting this low frequency was to achieve a high efficiency under modulation with acceptable capacitance at the input and output. In applications where capacitance reduction is desired, significantly higher modulation frequencies can be realized.

For the transformation stage, the reactive elements values were chosen considering the tradeoffs between the losses in the parasitics of the transformer, the matching network, and the RCN. If the total gain provided by the transformer and matching network is increased, the magnitude of impedance of the RCN also has to be increased. This helps in reducing the increase

in output power at higher output voltages, which in turn helps maintain high efficiencies at the higher output voltages. If more gain is provided by the matching network, the value of the matching network inductance increases, and thus, the matching network loss also increases. However, this results in a decrease in the required gain of the transformer that can result in a decrease in transformer loss.

A tradeoff of the losses in the transformer and matching network was considered to determine the value of the gain of these elements. For the matching network, an achievable inductor Q was selected, and the results of [17] were used to compute the loss of the matching network for a range of matching network gain values. Each matching network gain results in a specified transformer gain. A computer search routine was then used to identify the best transformer design for each specified gain. Transformers were designed by searching fully across a set of specified cores and wire/foil configurations to minimize transformer loss (the code provided in [22], which uses the power loss equations given in the appendix, was used to estimate these losses). The split of gains (between matching network and transformer) and the transformer design leading to the lowest total computed loss were then selected. For available cores and wires, the transformer turns ratio (N) was chosen to be 6 and the gain of the matching network (G) was chosen to be 1.67, for a

total gain of approximately 10. It is noted that more sophisticated optimizations could yield better results. This could include fully optimizing the design of the matching network inductor as part of the search to cooptimize the transformer/matching-network system (e.g., to maximize the achievable overall efficiency in a given volume). Likewise, introduction of more sophisticated loss models could be expected to provide refined results. Nevertheless, the method utilized is efficient and yields good results.

The value of X_s was calculated using (3) with the output power set to a value of 200 W and input voltage set to its minimum value of 25 V and output voltage set to 400 V. This ensures output power of 200 W across the entire input voltage range. To ensure output power of 200 W across the entire output voltage range the maximum value of X_s needs to be selected with an input voltage set at 25 V, output power at 200 W and varying the output voltage from 250 to 400 V. The two values are very similar in this case as the RCN greatly reduces the variation in output resistance with change in output voltage. From this, the value of L_s and C_s were obtained using $L_s = X_s/\omega$ and $C_s = 1/\omega X_s$. The values of L_{rp} and C_{rp} were calculated using (4) and (6), which makes the input impedance of the matching network resistive. However, the value of L_{rp} was increased slightly to provide slightly inductive loading of the inverter to achieve ZVS switching of the inverter switches.

V. SIMULINK RESULTS

The RCN dc/dc converter has been tested using a dc power supply and a dc motor chopper drive.
The tests were carried out and the results of output load with different input voltages (in the 25–40 V range) and different output voltages (in the 250–400 V range). Fig. 11 shows current and voltage waveforms for the converter over two switching periods, when operated at an input voltage of 25 V. In particular, it shows the current through the inductor of the matching network, which is also the output current of the inverter, the gate drive voltages of the inverter switches S_1 and S_3, and the drain–source voltage of the switch S_3. As expected, the current through

the inductor of the matching network is approximately sinusoidal. Also, the switches achieve ZVS and near-ZCS, as can be seen from Fig. 12. Even with the slight distortion in currents that occur owing to limited tank Q, ZVS, and near-ZCS is still achieved as predicted with sinusoidal approximations. This owes in part to the fact that even with moderate damping of the resonant oscillation owing to the rectifier network, the current waveform still tends toward zero (at a reduced slope) for the next switching transition. Fig. 12(a) shows a zoomed in view of the turn-off transition of switch S_3. The current through switch S_3 at turn-off is small compared to both the peak and average of the current it carries (turn-off current is 15.7% of peak current and 27.5% of average current). Fig. 12(b) shows the turn-on transition of switch S_3. Notice that the switch turns ON under ZVS, as the voltage across the switch falls to zero before the switch is turned ON. Fig. 13 shows the current and voltage waveforms with an input voltage of 40 V and an output voltage of 400 V.
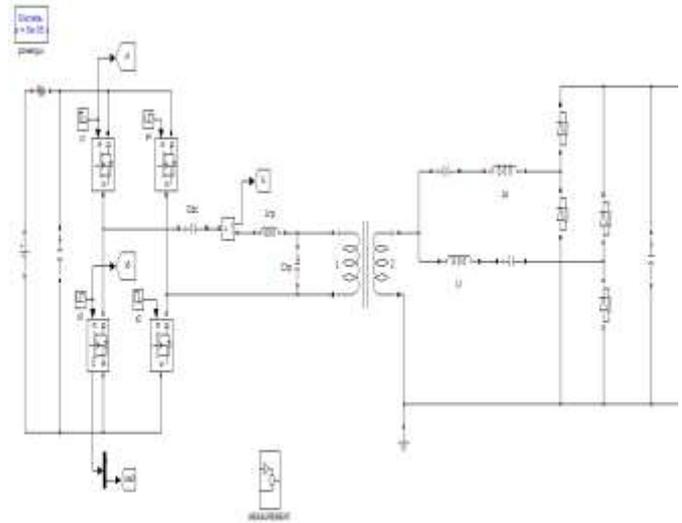
Fig:- simulink type RCN dc/dc converter
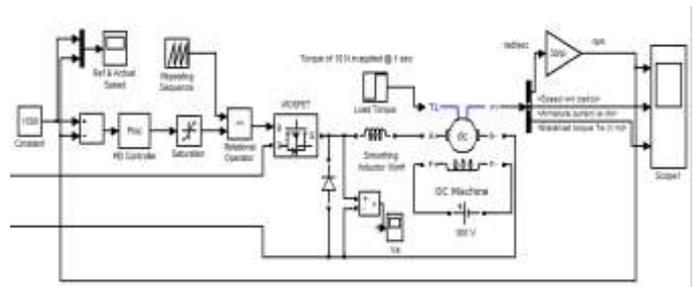
Fig.-simulink type chopper DC drive with fixed ref speed
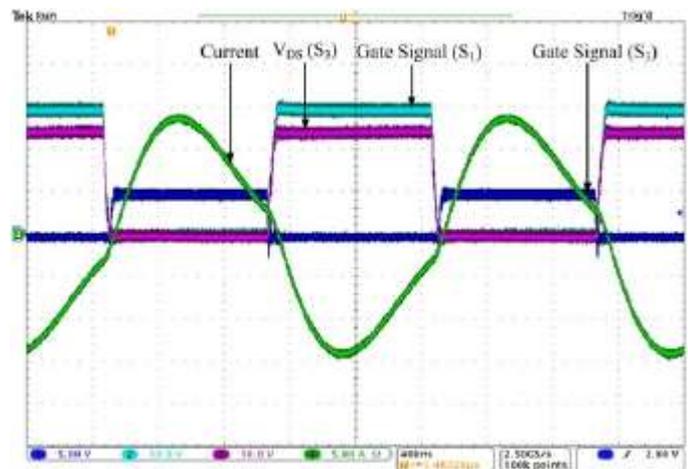
Fig. 11. Current and voltage waveforms of the RCN dc/dc converter when operated at an input voltage of 25 V: (1-blue) Gate voltage of switch S_3, (2-turquise) gate voltage of switch S_1, (3-magenta) drain–source voltage of switch S_3, and (4-green) current through inductor of the matching network.

(a)

(b)

Fig. 12.   Current and voltage waveforms of the RCN dc/dc converter when operated at an input voltage of 25 V, showing (a) turn-off transition and (b) turn-on transition. (1-blue) Gate voltage of switch S_3, (2-turquoise) gate voltage of switch S_1, (3-magenta) drain–source voltage of switch S_3 and (4-green) current through inductor of the matching network. Zero-voltage and near-zero-current switching is realized.

The converter was operated slightly off resonance at 425 kHz switching frequency to decrease the instantaneous output power at the increased input voltage. This off resonance operation results in a slight distortion of the current waveform as can be seen in Fig. 13. However, the converter still maintains ZVS and near-ZCS operation as the input impedance of the matching network still remains slightly inductive. The converter maintains near-ZCS operation over the entire input voltage and output voltage range. The highest current at switch turn-off is no more

than 13.6% of peak switch current (and 24.4% of average current) when the converter is operated at its nominal input voltage of 32.5 V; and when the input voltage is at its maximum of 40 V, the switch turn-off current rises to only 18.9% of peak switch current (and 50% of average current).

As illustrated earlier, narrow-range frequency operation is used to improve the overall performance of the converter. By adjusting the converter switching frequency over a narrow range from 425 to 500 kHz as input voltage varies, the maximum out-
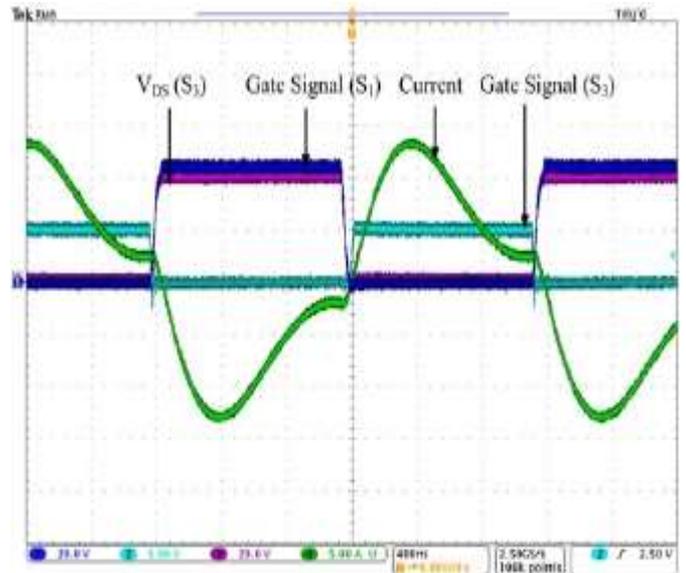
Fig. 13.   Current and voltage waveforms of the RCN dc/dc converter when operated at an input voltage of 40 V: (1-blue) gate voltage of switch S_1, (2-turquoise) gate voltage of switch S_3, (3-magenta) drain–source voltage of switch S_3, and (4-green) current through inductor of the matching network.

put power that can be delivered by the converter can be maintained within a narrower range than if strictly fixed-frequency operation is used, yielding moderate power variation across variations in input voltage. This helps maintain high efficiency as the input voltage varies. The switching frequency is decreased as the input voltage increased: 500 kHz is used at an input voltage of 25 V and 425 kHz with an input voltage of 40 V. The maximum output power then varies from 200 to 325 W across the full range of input voltage, with the output voltage at 400 V, as shown in Fig. 15(a). The converter can certainly be operating at fixed frequency over the complete input voltage range (for cases where absolute fixed-frequency operation is desired). However, this results in higher instantaneous output power at higher input voltages, as illustrated by the comparison of Fig. 14 (operation at fixed frequency) to Fig. 15 (operation with small frequency variation). Fig. 16 shows a comparison of the variation in instantaneous output power as a function of input voltage and output voltage at fixed switching frequency versus variable switching frequency). It can be seen that the use of modest frequency variation as the input voltage varies serves to reduce the effect of input voltage variations on converter operation.

The converter was also tested for output voltage variations from 250 to 400 V. When the output voltage is reduced from 400 to 250 V with input voltage held at 25 V (and switching frequency correspondingly held constant), the maximum output power varies over only a very narrow range, dropping slightly from 203 to 195 W, as shown in Fig. 15(b). It can be seen that the RCN is highly effective in suppressing the effects of output
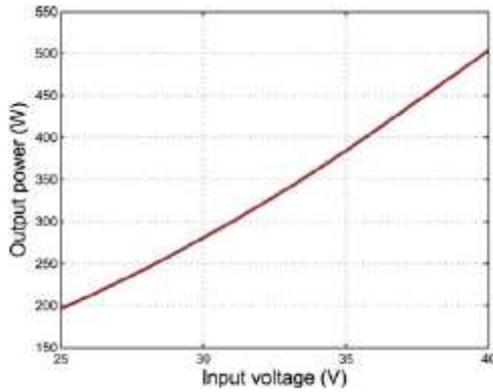
Fig. 14. Instantaneous output power with input voltage variation at fixed switching frequency of 500 kHz.
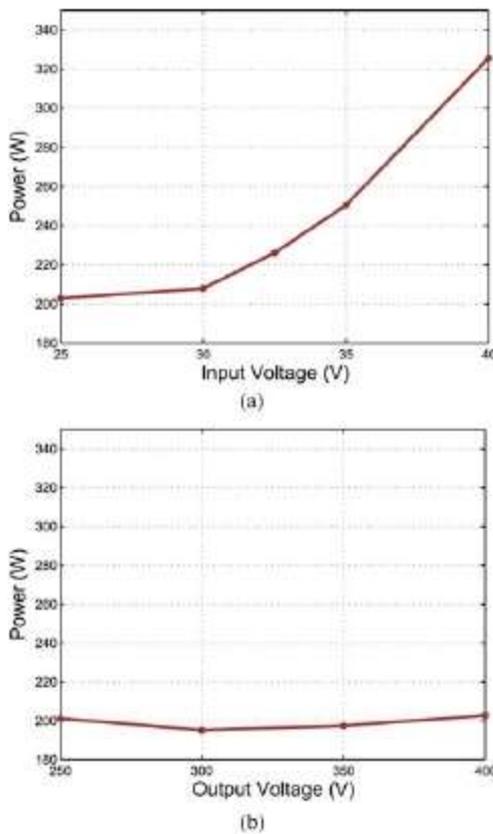
Fig. 15. Output power of the RCN dc/dc converter with (a) input voltage variation and (b) output voltage variation. The output power can be controlled below the levels indicated though ON–OFF control. Note the effectiveness of the RCN in suppressing the effects of output voltage variation on the operation (output power) of the converter.

voltage variation on the operation (e.g., instantaneous power) of the converter. By using the RCN to greatly limit the effects of output voltage variation, and narrow-range frequency control to moderately reduce the effects of input voltage variation, good performance over wide voltage operating ranges is achieved.

The efficiency of the RCN dc/dc converter was also measured across variations in input voltage, output voltage, and output power. The measured efficiency of the converter as a function of input voltage is plotted in Fig. 17. The converter maintains
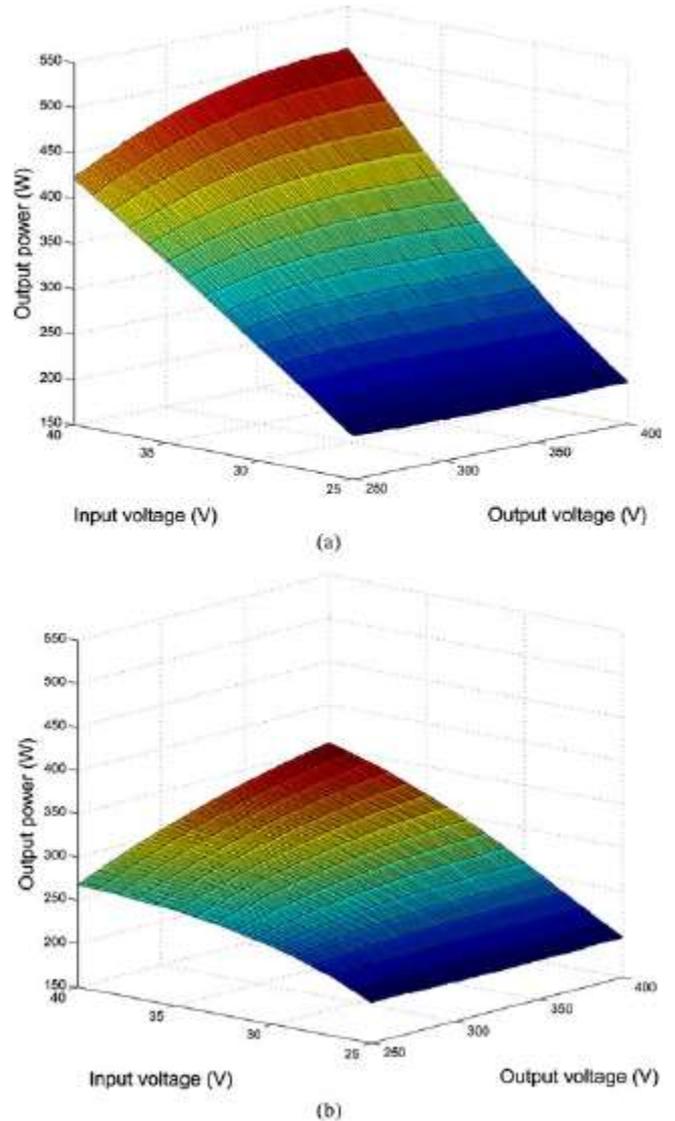
Fig. 16. Variation in output power of the RCN dc/dc converter as a function of input voltage and output voltage based on simulated results (a) under fixed (500 kHz) switching frequency operation, and (b) under narrow-range (425–500 kHz) switching frequency operation. While the RCN substantially suppresses variations in output power with changes in output voltage, there is a significant variation in power with changes in input voltage. The narrow-band frequency control helps reduce this power output.
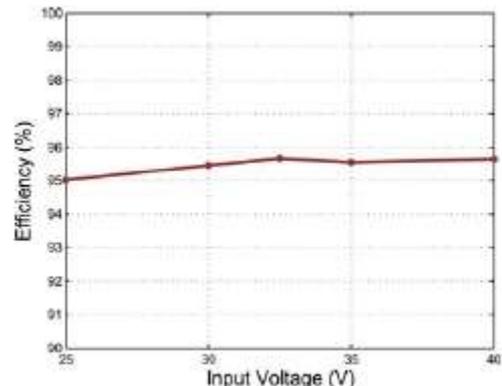
Fig. 17. Efficiency of the RCN dc/dc converter as the input voltage varies.
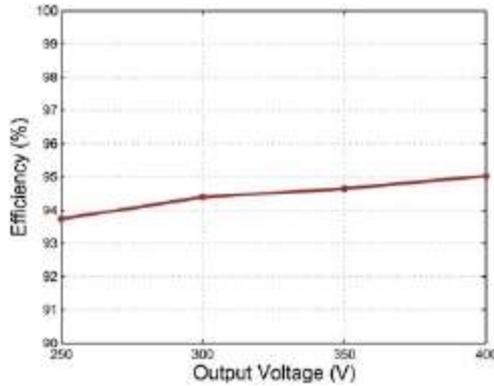
Fig. 18.   Efficiency of the RCN dc/dc converter as the output voltage varies.
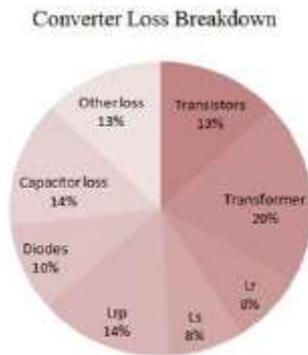
Fig. 19.   Estimated breakdown of converter losses. The "other loss" category includes board trace loss.

Fig. 20.   (4-green) Input current and (2-turquoise) input voltage of the matching network with 50% duty ratio of ON/OFF modulation.

(a)

(b)

Fig. 21.   (4-green) Input current and (2-turquoise) input voltage of the matching network with 50% duty ratio of ON/OFF modulation at (a) turn-on and (b) turn-off.

efficiency above 95% across the full range of input voltage. The efficiency of the converter increases from 95% to 95.6% as input voltage increases from 25 to 40 V. The efficiency of the converter as a function of output voltage is shown in Fig. 18. As the output voltage decreases from 400 to 250 V, with input voltage held constant at 25 V, the efficiency of the converter drops from 95% to 93.7%. The lower efficiency at the lower output voltage is due to the larger currents flowing through the output stages of the converter.

The loss mechanisms in this dc/dc converter were esti- mated using equations provided in the appendix and data from component datasheets. Fig. 19 shows the loss break down of the converter for an input voltage of 25 V, output voltage of 400 V, and output power of 200 W. More than 50% of the loss is due to the magnetic elements, with the transformer causing the largest amount of loss. Semiconductor losses are the next largest cat- egory, followed by capacitor losses. Board trace losses (under "other loss") can be reduced through appropriate board design.

The output power of the converter is controlled below its maximum value using ON/OFF control at an ON/OFFf modu- lation frequency of 500 Hz. The output power is determined by the duty ratio of the modulation command waveform. A 100% duty ratio delivers maximum power (roughly 200 W at 25 V) and a 10% duty ratio corresponds to 10% of maximum power (roughly 20 W at 25 V). Fig. 20 shows the current flowing into the matching network (I_i in Fig. 2) and the voltage at the in- put of the matching network (V_i in Fig. 2) when the converter

is operating with an ON–OFF modulation duty ratio of 50%. Fig. 21(a) shows these current and voltage waveforms when the converter turns ON. It takes around five cycles for the current to achieve steady state. Fig. 21(b) shows the same waveforms
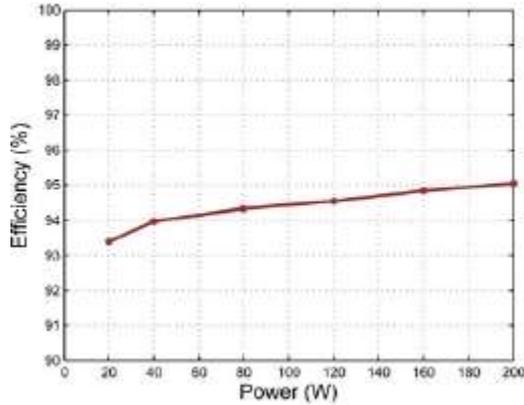
Fig. 22.   Efficiency of the RCN dc/dc converter as the output power is varied using ON/OFF control. This was measured with V_{in} = 25 V and V_{out} = 400 V.

when the converter turns OFF. It takes around 30 cycles for the current to drop down to 10% of the peak current value. The total output capacitance is 126.4 μF, which reduces the peak-to-peak output voltage ripple to less than 2% over the entire power range. For the input, a 5000-μF capacitor was used. As the power supply driving the converter has very high output capacitance, less than 1% peak-to-peak ripple was observed. However, without the power supply's output capacitance, in the worst case, around 12% peak-to-peak ripple would be observed. This is in the range of ripple often allowed for PV systems (e.g., at 120 Hz or other frequencies) in order to provide information for maximum power point tracking. Reduced ripple is readily achieved by increasing input capacitance and/or increasing modulation frequency.

The efficiency of the converter as a function of output power is shown in Fig. 22. With input voltage of 25 V and output voltage of 400 V, the efficiency varies from 95% to 93.4% as output power is reduced from full load (200 W) to 10% of full load (20 W). These results demonstrate that the proposed RCN dc/dc converter can maintain ZVS and near-ZCS operation and offer high efficiency across a wide input voltage, output voltage, and output power range.

PERFORMANCE WAVE FORMS OF A DC MOTOR DRIVE
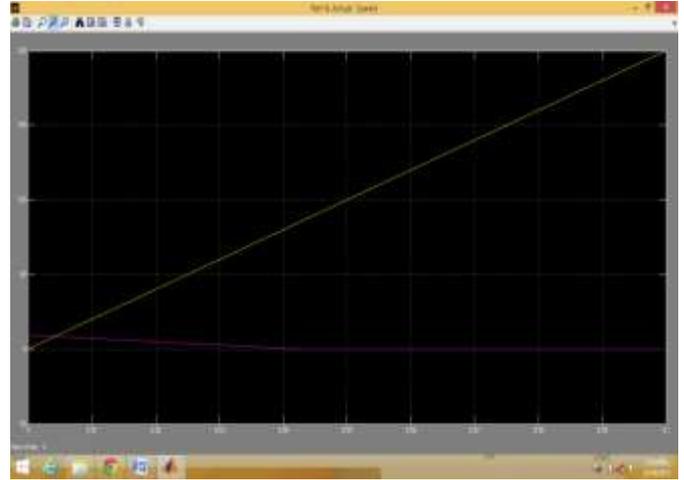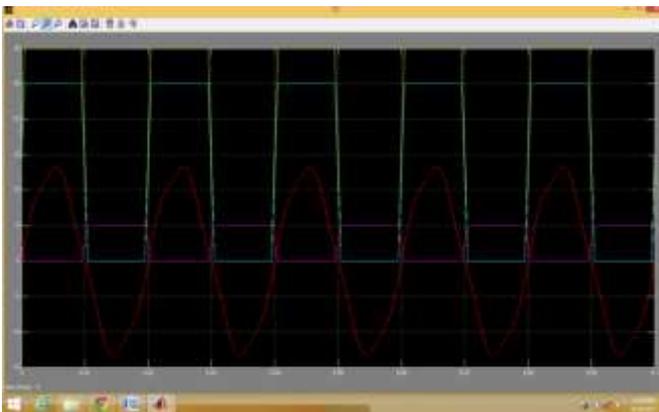
fig:-chopper dc motor drive actual and ref speed with clock

below fig:-speed, armature current and torque o/p of dc motor drive with ref clock i/n side
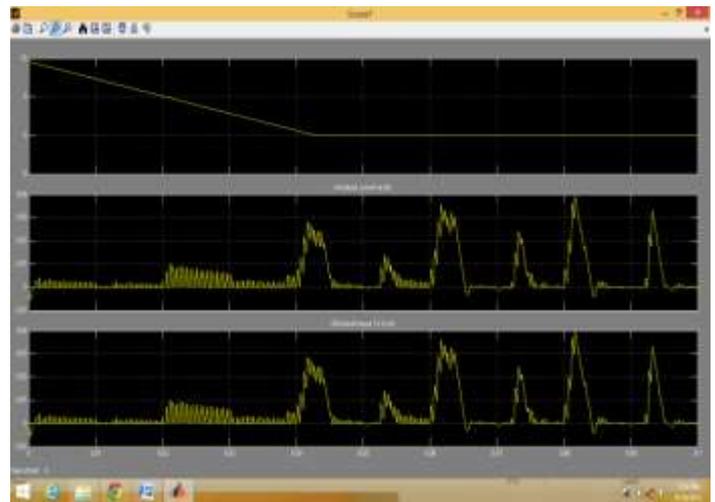
Fig:- RCN DC/DC converter output waveforms
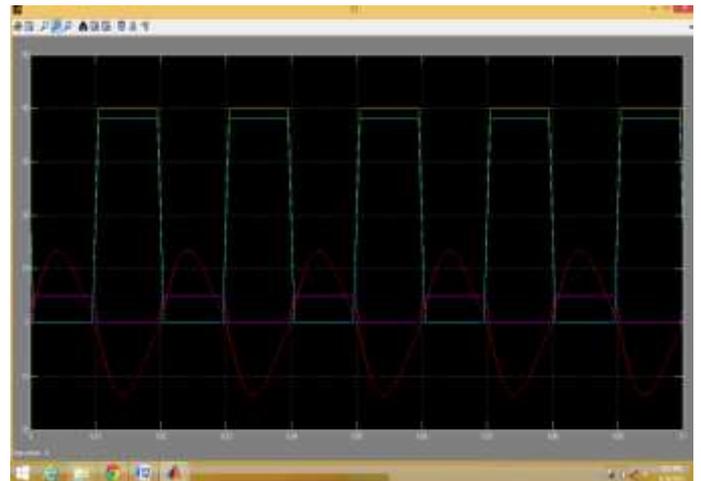
Fig:-reversing amplitudes switching of mosfets
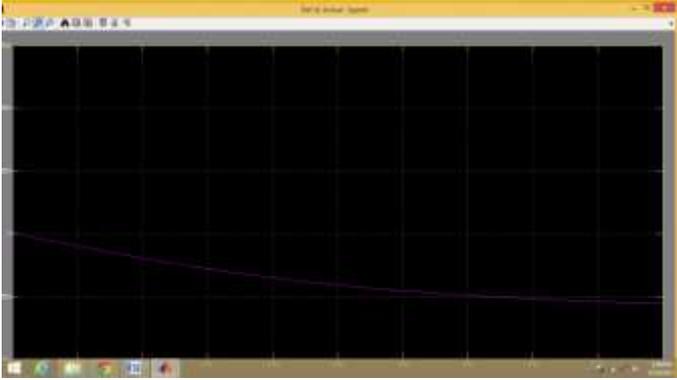
Fig:- chopper dc motor drive fixed ref speed(1500rpm) and

actual speed
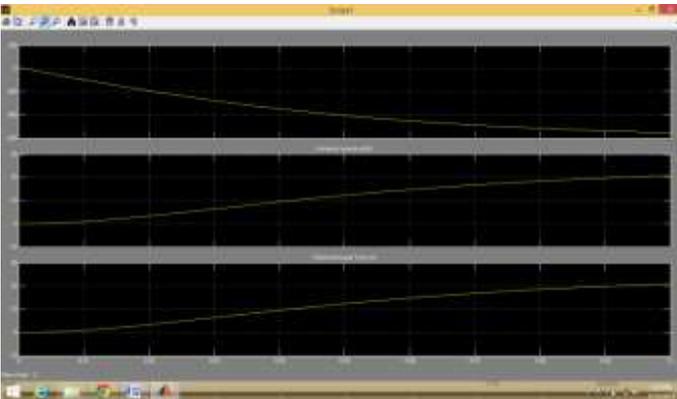
Fig:-chopper dc motor drive speed, amature current and

armature torque with fixed referance speed(1500rpm)

VI. CONCLUSION

This paper presents a new resonant dc/dc converter topology that uses an RCN and a combination of ON/OFF control and narrowband frequency control connected input of chopper dc motor drive   . The converter implementation
provides galvanic isolation and enables large (greater than 1:10) voltage conversion ratios. The proposed converter achieves very high efficiency by maintaining ZVS and near-ZCS over a wide input voltage, output voltage, and power range. The simulat ion results indicates the RCn network output waveforms and chopper dc motor drive peformance curves of speed,armature current and armature torque with variable clock referance speeds   and   fixed   referance   speeds from a 200-W show that the converter
maintains an efficiency of over 95% across its entire 25–40 V input voltage range at the designed output voltage of 400 V; an efficiency of over 93.7% as output voltage is reduced down to

250 V; and an efficiency of over 93.4% even as output power is redu ced to 20 W. I

$$P_{\text{cu-wire}} = I_{\text{rms}-w}^2 R_{\text{dc}} F_r \qquad (10)$$

n this present simulation output wave forms of dc motor drive   with speed,   armature current and armature torque

APPENDIX

LOSS ESTIMATION

This appendix provides the equations used to estimate the loss breakdown in the RCN converter presented in Section V. As the mosfets turn ON under zero voltage their turn-on loss is negligible. Hence, the losses in the mosfets are mainly conduction losses and turn-off losses. The conduction losses are estimated using the RMS current through each device and its on-state resistance. The turn-off losses are estimated assuming that the current through the mosfets decreases linearly to zero when the device is switched OFF. Hence, the current through the mosfet's output capacitance increases linearly resulting in a quadratic rise of voltage across the device. This overlap of current and voltage during the turn-off transition causes the loss. Thus, the losses in a mosfet are given by

$$P_{\text{tran}} = I_{\text{rms}}^2 R_{ds-\text{on}} + \frac{I_{\text{off}}^2 t_f^2 f}{24 C_{oss}}. \qquad (7)$$

TABLE III

PARAMETER VALUES OF 3F3 MATERIAL TO CALCULATE THE POWER LOSS

DENSITY

Parameter	Value
C_m	2×10^{-5}
x	1.8
y	2.5

$$P_{\text{core}} = C_m f^x B_{\max} V (c_{t0} - c_{t1} T + c_{t2} T^{\prime}) \qquad (9)$$

Where I_{rms} is the RMS current through the mosfet, $R_{ds-\text{on}}$ is its on-state resistance, I_{off} is the current through the mosfet at the instant when it is turned off, t_f is the fall-time of the current, f is the switching frequency, and C_{oss} is the output capacitance of the mosfet.The diode loss is given by

$$P_{\text{diode}} = I_{\text{rms}-d}^2 R_T + I_{\text{avg}-d} V_T \qquad (8)$$

where $I_{\text{rms}-d}$ is the RMS current through the diode, R_T is its on-state resistance, $I_{\text{avg}-d}$ is its average current, and V_T is its on-state voltage drop.

Losses in the magnetic components are comprised of the core losses and winding losses. The core losses are estimated as

$$P_{\text{cu-foil}} = I_{\text{rms}-f}^2 R_{\text{dc}} \frac{d}{\delta} \qquad (11)$$

C_m, x, y, c_{t0}, c_{t1}, and c_{t2} are parameters found by curve fitting the measured power loss data [24] and are given in Table III. Here B_{max} is the maximum flux density through the core, V is its effective volume, and T is the core temperature. The winding losses in the case of litz wire are estimated using

where I_{rms-w} is the RMS current through the wire, R_{dc} is the dc resistance of the wire, and F_r is a factor that relates the dc losses to the ac losses assuming the current is sinusoidal [25]. The winding losses in the case of copper foil are estimated using where $I_{rms-foil}$ is the RMS current through the foil, d is the width of the copper foil, and δ is the skin depth.

Finally, capacitor losses are estimated using

$$P_{cap} = I_{rms-c}^2 R_{ESR} \qquad (12)$$

where I_{rms-c} is the RMS current through the capacitor and R_{ESR} is its ESR.

REFERENCES

[0] High Efficiency Resonant DC/DC Converter Utilizing a Resistance Compression Network Wardah Inam, Student Member, IEEE, Khurram K. Afridi, Member, IEEE, and David J. Perreault, Fellow, IEEE, IEEE Transactions on power electronics, vol. 29, no. 8, august 2014.

[1] S. M. Chen, T. J. Liang, L. S. Yang, and J. F. Chen, "A cascaded high step-up dc/dc converter with single switch for microsource applications," *IEEE Trans. Power Electron.*, vol. 26, no. 4, pp. 1146–1153, Apr. 2011.

[2] S. V. Araujo, R. P. Torrico-Bascope, and G. V. Torrico-Bascope, "Highly efficient high step-up converter for fuel-cell power processing based on three-state commutation cell," *IEEE Trans. Ind. Electron.*, vol. 57, no. 6, pp. 1987–1997, Jun. 2010.

[3] Q. Zhao and F. C. Lee, "High-efficiency, high step-up dcdc converters," *IEEE Trans. Power Electron.*, vol. 18, no. 1, pp. 65–73, Jan. 2003.

[4] B. York, W. Yu, and J. S. Lai, "An integrated boost resonant converter for photovoltaic applications," *IEEE Trans. Power Electron.*, vol. 28, no. 3, pp. 1199–1207, Mar. 2013.

[5] J. S. Lai, "Power conditioning circuit topologies," *IEEE Ind. Electron. Mag.*, vol. 3, no. 4, pp. 24–34, Jun. 2009.

[6] Q. Li and P. Wolfs, "A review of the single-phase photovoltaic module integrated converter topologies with three different DC link configurations," *IEEE Trans. Power Electron.*, vol. 23, no. 3, pp. 1320–1333, May 2008.

[7] R. L. Steigerwald, "A comparison of half-bridge resonant converter topologies," *IEEE Trans. Power Electron.*, vol. 3, no. 2, pp. 174–182, Apr. 1988.

[8] B. Sanzhong, Z. Pantic, and S. Lukic, "A comparison study of control strategies for ZVS resonant converters," in *Proc. IEEE 36th Annu. Conf. Ind. Electron. Soc.*, Nov. 2010, pp. 256–262.

[9] B. Sanzhong, Z. Pantic, and S. Lukic, "A comparison study of control strategies for ZVS resonant converters," in *Proc. IEEE 36th Annu. Conf. Ind. Electron. Soc.*, Nov. 2010, pp. 256–262.

[10] R. T. H. Li, M. F. Vancu, F. Canales, and D. Aggeler, "High performance dc-dc converter for wide voltage range operation," in *Proc. 7th Int. Power Electron. Motion Control Conf.*, Jun. 2012, vol. 2, pp. 1151–1158.

[11] J. P. Vandelac and P. D. Ziogas, "A DC to DC PWM series resonant converter operated at resonant frequency," *IEEE Trans. Ind. Electron.*, vol. 35, no. 3, pp. 451–460, Aug. 1988.

[12] P. K. Jain, A. St-Martin, and G. Edwards, "Asymmetrical pulse-width-modulated resonant DC/DC converter topologies," *IEEE Trans. Power Electron.*, vol. 11, no. 3, pp. 413–422, May 1996.

[13] Y. S. Lee and Y. C. Cheng, "A 580 kHz switching regulator using on-off control," *J. Inst. Electron. Radio Eng.*, vol. 57, no. 5, pp. 221–226, Sep./Oct. 1987.

[14] W. Inam, K. K. Afridi, and D. J. Perreault, "High efficiency resonant dc/dc converter utilizing a resistance compression network," in *Proc. IEEE Appl.*

Power Electron. Conf. Expo., Mar. 2013, pp. 1399–1405.

[15] Y. Han, O. Leitermann, D. A. Jackson, J. M. Rivas, and D. J. Perreault, "Resistance compression networks for radio-frequency power conversion," *IEEE Trans. Power Electron.*, vol. 22, no. 1, pp. 41–53, Jan. 2007.

[16] P. A. Godoy, D. J. Perreault, and J. L. Dawson, "Outphasing energy recovery amplifier with resistance compression for improved efficiency," *IEEE Trans. Microw. Theory Tech.*, vol. 57, no. 12, pp. 2895–2906, Dec. 2009.

[17] Y. Han and D. J. Perreault, "Analysis and design of high efficiency matching networks," *IEEE Trans. Power Electron.*, vol. 21, no. 5, pp. 1484–1491, Sep. 2006.

[18] J. M. Rivas, R. S. Wahby, J. S. Shafran, and D. J. Perreault, "New architectures for radio-frequency DC–DC power conversion," *IEEE Trans. Power Electron.*, vol. 21, no. 2, pp. 380–393, Mar. 2006.

[19] R. C. N. Pilawa-Podgurski, A. D. Sagneri, J. M. Rivas, D. I. Anderson, and D. J. Perreault, "Very-high-frequency resonant boost converters," *IEEE Trans. Power Electron.*, vol. 24, no. 6, pp. 1654–1665, Jun. 2009.

[20] J. M. Rivas, O. Leitermann, Y. Han, and D. J. Perreault, "A very high frequency DC–DC converter based on a class $\varphi 2$ resonant inverter," *IEEE Trans. Power Electron.*, vol. 26, no. 10, pp. 2980–2992, Oct. 2011.

AUTHORS

B.UMAMAHESWARA RAO received his B.Tech degree in Electrical and Electronics Engineering from Audisankara College Of Engineering and Technology, Gudur, Nellore dist, affiliated to JNTU Hyderabad He is currently pursuing M.Tech power electronics in Brahmaiah college of engineering, northrajupalem, SPSR Nellore (Dist), affiliated to JNTU Anantapur,

P.SIVA KRISHNA received his B.Tech Degree in Electrical and Electronics Engineering from Narayana engineering college, Nellore affilated to jntu ananthapur. He received his M.Tech from sree venkataperumalu engineering college puttur,chitter dist. He has 1 years teaching experience, presently working as Professor of EEE, Brahmaiah college of engineering Affiliated to JNTU, Anantpur. Andhra Pradesh, India